LUOJIA Explorer: An Auto-UAV for Unexposed Space Exploration

Shangzhe Sun[1,2,3], Chi Chen[1,2,3,*], Bisheng Yang[1,2,3], Liuchun Li[4], Yuhang Xu[1,2,3], Ang Jin[1,2,3]

[1] State Key Laboratory of Information Engineering in Surveying, Mapping and Remote Sensing, Wuhan University, Wuhan, China – (SSZ, chichen, bshyang, yuhangxu, angjin)@whu.edu.cn
[2] Engineering Research Center for Spatio-temporal Data Smart Acquisition and Application, Ministry of Education of China, China
[3] Institute of Artificial Intelligence in Geomatics, Wuhan University, Wuhan, China
[4] Institute of Artificial Intelligence, School of Computer Science, Wuhan University, Wuhan, China – LiuC.Lee@whu.edu.cn

Keywords: UAV, Unexposed Space, SLAM, Planning, Automation, Exploration.

Abstract

With the advancement of technology, unexposed spaces have emerged as a new type of strategic area, attracting significant attention from researchers. These spaces often present complex environments, such as extreme lighting variations, irregular geometries, and the lack of external positioning signals, making human entry hazardous. Fortunately, advancements in robotics and artificial intelligence have enabled unmanned systems to mitigate these challenges, allowing for safer exploration of unexposed spaces. UAVs, as vital unmanned system platforms, are extensively used across various industrial scenarios and are particularly effective for detecting unexposed spaces. To facilitate automated exploration of these areas, we propose the autonomous UAV system, LUOJIA Explorer. Equipped with a LiDAR sensor, data transmission module, and external anti-collision devices to protect the aircraft, LUOJIA Explorer is designed for effective unexposed space detection. We have integrated a laser point cloud positioning and mapping subsystem, along with a planning and control subsystem, into the LUOJIA Explorer. Through both simulation and actual experiments, the Luojia Explorer has demonstrated the capability to achieve stable flight based on self-positioning in unexposed spaces, with an exploration efficiency of 88.83 m³/s.

1. Introductions

Unexposed space is a type of space that is closely related to human activities and includes underground spaces, indoor spaces and other spaces that are not open to the outside world. While it is often characterised by a complex environment, large light changes, poor passability, feature degradation and signal denial, which pose challenges for human beings to carry out productive activities(Rouček et al., 2020). Unexposed space surveying means a lot for people. By precisely surveying unexposed space such as underground space and so on, people can obtain space information for further application. For a long time, researchers have concentrated on measuring and modelling external space, often overlooking unexposed spaces, which are a significant resource. Furthermore, indoor space is one kind of important unexposed space. The precise measurement of interior spaces is crucial. Accurate measurements of indoor and other non-exposed areas are of great significance for smart cities, emergency evacuations, fire protection, and more(Cui et al., 2023). Underground space is a crucial type of non-exposed area. Accurate measurement of non-exposed spaces, such as urban underground space (UUS), can help alleviate urban resource scarcity, enhance environmental conditions, and improve residents' quality of life(Yu et al., 2023). In addition, data acquisition technology for studying naturally occurring non-exposed spaces, such as karst caves, can provide a technical basis for geological research(Sauro et al., 2020) and extraterrestrial lava tube detection(Xiao et al., 2018).

Although the exploration of non-exposed spaces is of great significance, it faces challenges such as limited terrain conditions and difficulties in data and information collection(Lai et al., 2023). Unmanned systems are a crucial technical means for gathering data and information in non-exposed spaces like underground areas. Common unmanned systems include platforms with various motion modes, such as unmanned aerial vehicles (UAVs), unmanned ground vehicles, and quadruped robots, which are used for detecting unexposed spaces. However, the complex terrain in non-exposed spaces can be challenging for unmanned ground vehicles, and quadruped robots may also face limitations due to their size. In such situations, drones have distinct advantages; their unique motion capabilities and small size allow them to navigate through spaces with poor traffic conditions where other unmanned vehicles cannot pass.

As an important aerial platform, UAVs have been widely used in various fields due to their unique motion modality and data acquisition perspective(Chen et al., 2022; Cheng et al., 2023; Deng et al., 2018; Sun et al., 2023). And with the rapid development of artificial intelligence(Hunt, 2014), computer vision and robotics(Al-Kaff et al., 2018), the degree of intelligence of UAVs has been further improved, which can be used for unexposed space exploration, but it also faces signal denial and complex positioning(Adamkiewicz et al., 2022). In unexposed spaces, developing UAV self-positioning and planning algorithms can enable the UAV to fly autonomously, eliminating the need for human control. However, due to limitations in visual sensors(Zhou et al., 2021; X. Zhou et al., 2020), current autonomous UAV systems have a small field of view, leading to instability in the autonomous detection of non-exposed spaces.

To realize unmanned intelligent exploration of unexposed space, we propose an intelligent UAV system, LUOJIA Explorer UAV, which realizes autonomous positioning, planning and mapping algorithms for unexposed space exploration based on solid-state LiDAR data, providing a new solution for unmanned exploration of unexposed space.

2. Related Work

Autonomous UAVs for exploring non-exposed spaces primarily involve unmanned aerial systems, SLAM (Simultaneous Localization and Mapping), and planning algorithms.

* Corresponding author

2.1 UAV System

Rotary-wing unmanned aerial vehicles (UAVs) have gained attention due to their flight characteristics, including stability, agility, and hovering capabilities. With the advancement of technology, the performance of rotary-wing UAVs has become increasingly stable. As a result, they are gradually transitioning from military applications to specialized and civilian applications, integrating into all aspects of production and daily life, and opening up a vast market. Several UAV enterprises have already developed a comprehensive production mode and produced a variety of quadcopter products to meet different needs. Examples of such enterprises include DJI, Daotong Intelligence, and Parrot, which specialize in producing rotor UAVs. Additionally, academic institutions have also produced rotor UAVs(Chen et al., 2023; Kong et al., 2021; Mohta et al., 2018; Tang et al., 2023; Tranzatto et al., 2022) (Zhou et al., 2022)for scientific research purposes. These UAVs serve as carriers for scientific research tasks and are used to conduct validation experiments.

2.2 SLAM

Many filter-based methods use the traditional Extended Kalman filter (EKF)(Bloesch et al., 2015), the Unscented Kalman Filter UKF(Wan, n.d.), or the improved Multi-State Constraint Kalman Filter(MSCKF)(Abdollahi et al., n.d.).

Back in 2007, the University of Minnesota proposed a visual inertial navigation framework called MSCKF(Mourikis and Roumeliotis, 2007), which is based on Extended Kalman Filtering. This framework extracts FAST feature points and tracks them using the KLT optical flow algorithm at the front end. At the back end, it uses EKF filtering for state estimation. In 2015, the Autonomous Systems Laboratory (ASL) of ETH Zurich proposed a monocular visual inertial odometry ROVIO based on Iterative Extended Kalman Filtering (IEKF)(Bloesch et al., 2015).

Currently, the field is dominated by optimization-based methods. These methods heavily rely on image filtering, feature extraction, and matching. In 2015, the Autonomous Systems Laboratory (ASL) at ETH Zurich proposed the OKVIS(Leutenegger et al., 2015), a keyframe-based visual inertial odometer that uses nonlinear optimization. The optimization is restricted to a bounded window of keyframes through marginalization to ensure real-time operation. The probabilistic cost function constructed includes both the reprojection error of landmarks and the inertial term. In 2017, Mur-Artal et al. proposed a tightly coupled monocular vision inertial SLAM system(Mur-Artal and Tardos, 2017) that utilizes closed-loop detection and map reuse to significantly improve the performance of SLAM systems in revisited areas. Thanks to this system, zero-drift localization is achieved in previously mapped areas, and centimeter-level accuracy is achieved on UAV-collected EuRoC datasets. Stumberg et al. proposed a direct method for visual-inertial odometry (VI-DSO) (von Stumberg et al., 2018), which incorporates scale and gravity direction into the model for joint optimization.

In addition to vision sensors, LiDAR is also a very popular sensor, because of its ability to directly obtain the 3D point cloud of the surrounding environment. Loosely coupled approaches to laser inertial odometry dominated the early laser inertial odometry methods due to their low computational cost and simple system structure. The classic loosely coupled laser inertial measurement method LOAM(Zhang and Singh, 2014), proposed by Carnegie Mellon University, extracts the effective edge and plane feature point information from the laser point cloud data, and then constructs the error function by using the distance from the point to the line and plane to solve the nonlinear optimization problem of the position, and then uses the integral operation of the six-axis IMU measurements to obtain the a priori position, which further improves the accuracy of the LiDAR odometer, but there is no closed-loop detection and optimization at the back-end of LOAM. Patrick Geneva et al. proposed a laser inertial SLAM method using planar features-LIPS (Geneva et al., 2018) at IROS2018, which is based on the graph optimization framework and proposes a nearest-point planar representation that parameterizes a set of point clouds into planar features, and then converts the residual function into the difference between the planar parameters of the two frames, which together with the residual term of the IMU pre-integration constitutes the final optimization function, which has been applied in both simulation and real experiments. Cedric Le Gentil et al. presented IN2LAMA (Gentil et al., 2019) at ICRA2019, which uses the pre-integration of the IMU to eliminate motion aberrations in the original point cloud, and jointly optimizes the IMU and LIDAR measurements together.

2.3 Planning

Yi Lin et al(Lin et al., 2018) used monocular vision inertial odometry for UAV self-localisation and an online trajectory planner for local planning on a UAV equipped with a fisheye camera and IMU to achieve autonomous navigation of a UAV in complex indoor and outdoor environments. In response to the case of serious aircraft failure during the planning process, Sihao Sun et al. proposed a planning and control method when paddle stall occurs during UAV flight(Sun et al., 2020), using a depth camera and an event camera.Boyu Zhou et al. proposed a replanning method(B. Zhou et al., 2020) that systematically solves the problem of the existence of local minima in gradient-based trajectory optimisation. A topological path search algorithm was developed to capture a collection of different useful paths in a 3D environment, and then each path guides an independent trajectory optimisation. It activates a more comprehensive exploration of the solution space and is able to output superior replanned trajectories. In order to solve the high-speed navigation problem of UAVs, Boyu Zhou et al. also proposed RAPTOR(Zhou et al., 2021), which is a perceptually based replanning framework to support fast and safe flights, which designs a path-guided optimisation method including multiple topological paths to ensure that feasible and high-quality trajectories are found in a very limited time, and also introduces a perceptually aware planning strategy to proactively observe and avoid unknown obstacles, which can ensure that UAVs observe unknown obstacles that may endanger themselves earlier and avoid them in time. Fei Gao et al. proposed a planning framework for aggressive flight of autonomous quadcopters(Gao et al., 2020).

3. System and Methods

3.1 Hardware System of LUOJIA Explorer UAV

The hardware system of LUOJIA Explorer UAV consists of a UAV450 frame, solid-state lidar, on-board processing unit, flight controller, motor, propellers, 6s model aircraft battery, data

transmission module, and anti-collision structure, as shown in Figure 1. The sensor details are shown in Table 1.

Figure.1 Hardware System of LUOJIA Explorer UAV

Sensors	descriptions
LiDAR	DJI Livox MID-360
data transmission device	transmit power from 100mW to 1W;902-928 MHz frequency band; Range up to 60km
IMU	Lidar built-in
Flight Control	Pix32 V6 mini

Table 1. Sensor Information.

3.2 Workflow of LUOJIA Explorer UAV

The system of LUOJIA Explorer UAV includes the positioning and mapping subsystem, the planning and control subsystem. The workflow is shown in Figure 2.

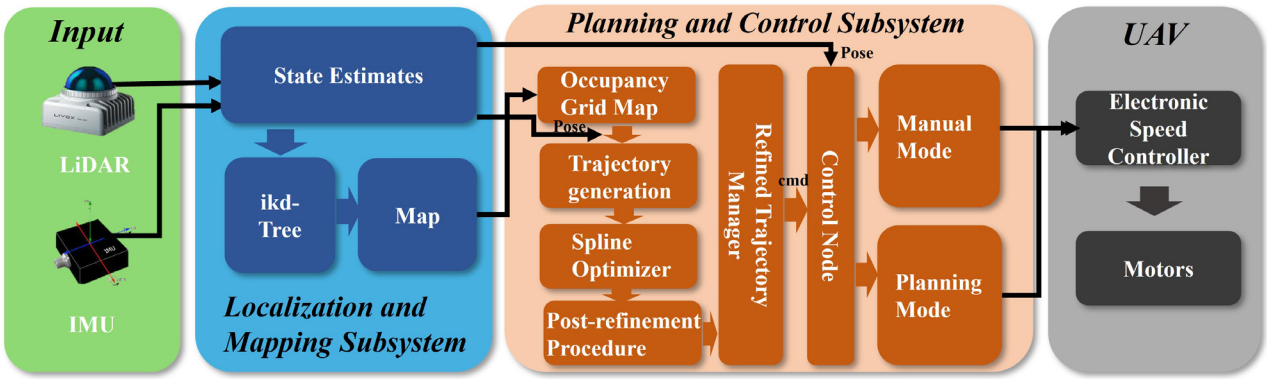

Figure.2 Workflow of LUOJIA Explorer UAV

3.2.1 Localization and Mapping Subsystem

The localization and mapping subsystem uses an iterative Kalman filter to process the point cloud and IMU data from the solid-state lidar to achieve robust localization in degraded unexposed environments while supporting fast and aggressive flight states.

The feature extraction module processes the LiDAR inputs to identify planar and edge features. These features, combined with IMU measurements, are subsequently used by our state estimation module, which performs state estimation at a rate of 10 Hz~50 Hz. The estimated pose then registers the feature points to the global frame and merges them with the feature points map built so far. The updated map is finally used to register further new points in the next step.

The Kalman gain calculation in Eq. (1) is used to achieve efficient computation during the state estimation process, which is based on the state dimension rather than the measurement dimension, thus avoiding the computation of a large number of measurements and significantly improving the computational efficiency. After derivation, Eq. (1) calculates the Kalman gain in the state dimension to achieve the same effect as the calculation in the measurement dimension, but can greatly reduce the amount of calculation. Where K is the Kalman gain, H is the Jacobi matrix associated with the state, R is the diagonal array of the external reference rotation parameters, and P is the covariance matrix.

$$K = (H^T R^{-1} H + P^{-1})^{-1} H^T R^{-1} \quad (1)$$

Instead of extracting the features of the point cloud data, the data processing stage directly uses the feature points in the environment together with the forward propagated IMU data to enter the state estimation process, which reduces the computational cost and improves the accuracy, thus directly registering the points to the map. In the map building part, an incremental k-d tree data structure is used to maintain the map, which realizes the incremental update and maintenance of the map. In order to provide the planning and control subsystem with a planning database, a distance-based thinning module has been added to the map building module to ensure the construction of stable navigation maps within neighbouring distances.

Initialization is essential for obtaining a reliable initial estimate of the system state, such as the gravity vector Gg, bias, and noise covariance, which in turn accelerates the state estimator. In localization and mapping subsystem, the initialization process is straightforward: keeping the LiDAR stationary for a few seconds (2 seconds in all the experiments described in this letter), the collected data is used to initialize the IMU bias and gravity vector. If the LiDAR supports non-repetitive scanning (e.g. Livox AVIA), remaining stationary also enables the LiDAR to create an initial high-resolution map, which is advantageous for subsequent navigation.

3.2.2 Planning and Control Subsystem

The planning and control subsystem first constructs an occupation grid navigation map based on the point cloud map after thinning, and then computes the optimal trajectory and

outputs control commands based on the current state estimation and the given target points.

The planning algorithm is a gradient-based local planning algorithm without Euclidean Symbolic Distance Field (ESDF). The Euclidean Symbolic Distance Field can quickly query the gradient and distance information in the obstacles, which is convenient for the planning algorithm to calculate the cost function in the re-optimization part, but the process of trajectory optimization only needs to update the information in the limited space within the range, so there are a lot of redundant calculations. We use a local planning framework without Euclidean symbolic distance fields, which is achieved by generating the collision penalty term in the penalty function by constantly comparing the trajectories that have collisions with the collision-free bootstrap paths, and storing the resulting obstacle information only when the generated trajectories encounter new obstacles. In the trajectory generation section, the classical A* algorithm is used to generate the initial trajectory. In the trajectory optimization section, a penalty function $\mathcal{T}_t$ consisting of a smoothing penalty term $\mathcal{T}_s$, a dynamic feasibility term $\mathcal{T}_d$, and a collision penalty term $\mathcal{T}_d$ is constructed to continuously optimize the generated trajectory by minimizing the penalty function. A time reallocation strategy is also incorporated into the back-end part of the trajectory planning to make the generated trajectories satisfy the dynamics of the unmanned system platform.

$$\mathcal{T}_t = \mathcal{T}_s + \mathcal{T}_d + \mathcal{T}_c \tag{2}$$

A smoother trajectory enhances the stability of the unmanned system during execution, conserves energy, and extends operating time. To achieve a smooth trajectory, a smoothing penalty is applied. Due to the convex hull property of B-splines, ensuring the smoothness of the initialized B-spline requires that the control points maintain small second and third derivatives. This guarantees that the overall B-spline curve's derivatives remain minimal, ensuring smoothness. In Eq. (3), $\mathbf{A}_i$ represents the second derivative (acceleration) of the B-spline control point, while $\mathbf{J}_i$denotes the third derivative (the derivative of acceleration) of the B-spline control point.

$$\mathcal{T}_s = \sum_{i=1}^{N_c-2} \|\mathbf{A}_i\|_2^2 + \sum_{i=1}^{N_c-3} \|\mathbf{J}_i\|_2^2 \tag{3}$$

When the unmanned system moves, it must adhere to its dynamic constraints, ensuring that the generated trajectory meets this fundamental requirement. This guarantees that the speed and acceleration in each dimension of motion remain within acceptable limits. For dynamic feasibility, it is necessary to restrict only the higher-order derivatives in each dimension of the trajectory. Similar to the smoothing penalty term, the derivatives of the trajectory's control points are also constrained. The dynamic feasibility penalty term is defined as shown in equation (4), where $\mathbf{V}_i$, $\mathbf{A}_i$, and $\mathbf{J}_i$ representssss the first-order derivative (velocity), second-order derivative (acceleration), and third-order derivative (jerk) of the control point, respectively. $F(\cdot)$ is a quadratic, continuously differentiable metric function of the higher-order derivatives of the trajectory control point, used to constrain $\mathbf{V}_i$, $\mathbf{A}_i$ and $\mathbf{J}_i$ within the dynamics-compliant range.

$$\mathcal{T}_d = \sum_{i=1}^{N_c-1} \omega_v F(\mathbf{V}_i) + \sum_{i=1}^{N_c-2} \omega_a F(\mathbf{A}_i) + \sum_{i=1}^{N_c-3} \omega_j F(\mathbf{J}_i) \tag{4}$$

The collision penalty term is a crucial part of the algorithm, ensuring that the trajectory effectively avoids obstacles. This penalty generates a simulated thrust to move the trajectory away from obstacles into a safe space. When the trajectory encounters an obstacle, the A* search algorithm is used to find two points on the trajectory outside the obstacle. Tangents and planes are created through point Q, which is located between these two points. The point p and the unit vector v are determined on the obstacle; v points to the intersection of the path found by the A* algorithm with the tangent at point Q, and p is the intersection with the obstacle in the direction of vector v. Points p and vector v are essential for determining whether the trajectory collides with the obstacle. The collision penalty term is defined in Eq. (4), where N_c is the number of obstacles in the trajectory, N_p is the number of p,v pairs, and $j_c(.)$ is a quadratically continuous differentiable penalty function used to impose specific limits on p and v to ensure no collisions occur.

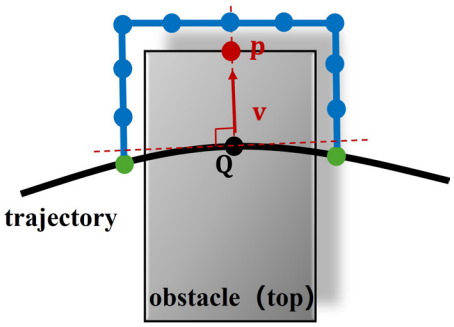

Figure 3. Collision Trajectory Generation

$$\mathcal{T}_c = \sum_{i=1}^{N_c} j_c(\mathbf{Q}_i) = \sum_{i=1}^{N_c} \sum_{j=1}^{N_p} j_c(i,j) \tag{5}$$

In the control part of the UAV, we send the state information output from the laser inertial odometer directly to the UAV flight control to obtain the current position information of the UAV, and then construct a control node supporting two control modes, which can support both manual control mode and planning control mode, to realize the one-button switching of the control mode of the UAV to ensure the stability of the flight.

4. Experiment and Results

We have conducted simulation experiments and real aircraft experiments, respectively.

In both simulation and live scenarios, our proposed LUOJIA Explorer UAV achieves stable autonomous flight. One of the simulation experiments was conducted in an unexposed space without GNSS.

4.1 Simulation Experiment

Using one of the outdoor environments in XTDrone(Xiao et al., 2020), we conducted simulation experiments in a software-in-the-loop manner. In the simulation environment, the UAV is unable to receive GNSS signals, so its local position is determined solely through our proposed positioning and mapping subsystem. To ensure the UAV can fly normally in this environment, the odometry data obtained by our algorithm is fed into the aircraft's flight controller. Figure 4 shows a screenshot of

the UAV flying autonomously in the simulation environment, while Figure 5 displays a point cloud map of the same environment. Our experiments in this simulation setting demonstrate that the proposed system can achieve stable autonomous flight even in the absence of GNSS signals. The UAV relies on the positioning and mapping subsystem we developed, which ensures accurate localization and navigation. These results underscore the effectiveness of our approach in maintaining autonomous UAV operation under challenging conditions.

Figure 4. Simulation Environment

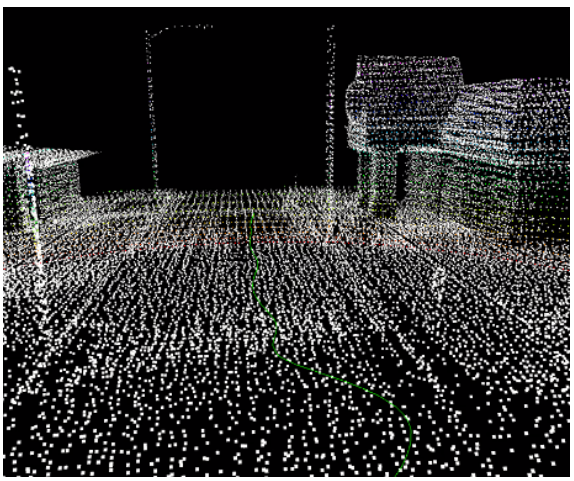

Figure 5. Point Cloud Map in Simulation Environment

4.2 Real Experiment

The real flight experiments were conducted on the fifth floor of the Star Lake Comprehensive Experiment Building of the Department of Informatics, Wuhan University, also without GNSS and other external positioning signals, and the LUOJIA Explorer UAV was able to fly and build maps in a stable manner. The unexposed space test site is 6.28 m long, 4.74 m wide and 3 m high as shown in the Fig. 6. We conduct a flight test at the test site, and it takes only 15 seconds to autonomously fly to the target point while avoiding obstacles, and at the same time, it takes only about 1 second to complete the construction map of the experimental site, and the exploration efficiency reached 88.83 m^3/s. The experimental results are shown in Table 2. Figure 7 shows a screenshot of the UAV in flight, while Figure 8 displays the established point cloud map and obstacle grid map.

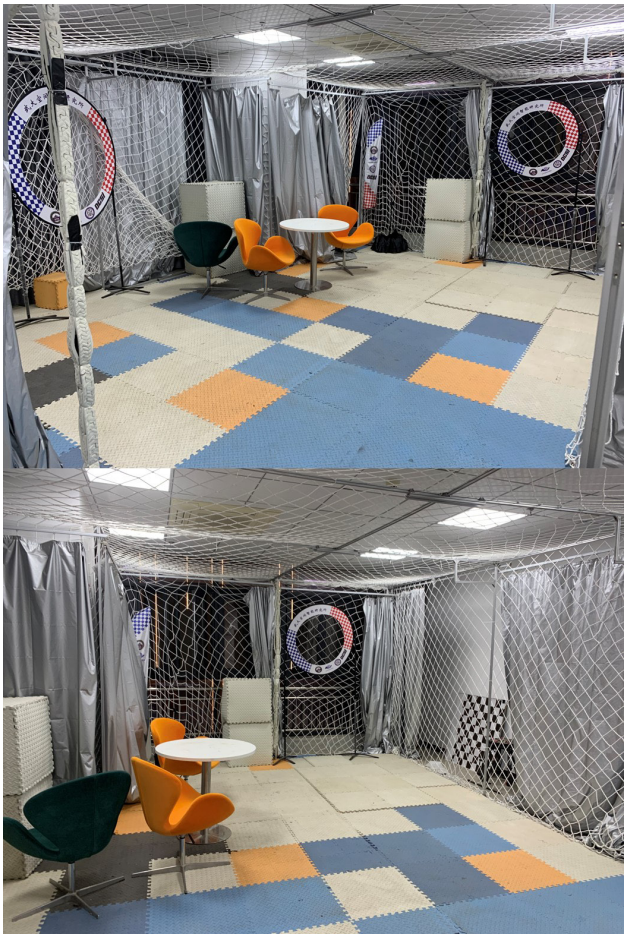

Figure 6. Real Environment

Figure 7. Real Flight

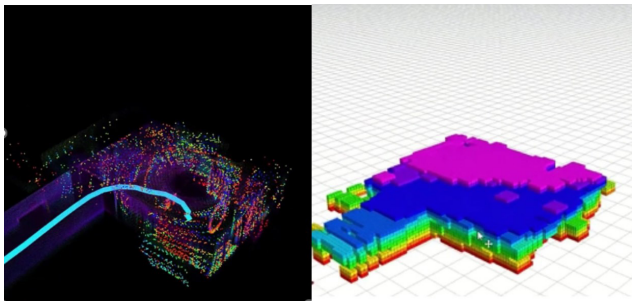

Figure 8. Real Cloud Point Map and Occupy Grid Map

Test Site Size(m)	Flight Time(s)	Exploration Efficiency(m^3/s)
6.28 ×4.74 ×3	15.32	88.83

Table 2. Quantitative Results.

5. Conclusion and Future Work

We propose LUOJIA Explorer UAV, an autonomous UAV based on solid-state LiDAR that can be used for unexposed space exploration. LUOJIA Explorer UAV consists of two subsystems: localization and mapping, and planning and control. The localization and mapping subsystem is a laser inertial odometer based on distance dilution, which can provide the planning algorithm with point cloud maps and state information. The planning and control subsystem greatly improves the planning efficiency by using an ESDF-free trajectory optimization method; the control node supports two control modes. The experimental results show that LUOJIA Explorer UAV can provide a robust solution for unexposed space exploration and offers new opportunities for air-ground cooperative exploration. In the actual test site, measuring 6.28 m in length, 4.74 m in width, and 3 m in height, an exploration efficiency of 88.83 m^3/s was achieved. In the future, we plan to expand autonomous UAS capabilities to include target-based exploration, enabling a broader range of real-world applications.

Acknowledgements

This research was funded by the National Natural Science Foundation of China (No.U22A20568), the National Key RESEARCH and Development Program (No.2022YFB3904101), the National Natural Science Foundation of China (No.42071451), the National Natural Science Foundation of China (No.42130105), the European Union’s Horizon 2020 Research and Innovation Program (No.871149), the National Natural Science Foundation of Hubei China (No.2022CFB007), the Key RESEARCH and Development Program of Hubei Province (No.2023BAB146), the Research Program of State Grid Corporation of China (5500-202316189A-1-1-ZN), the Fundamental Research Funds for the Central Universities, the China Association for Science and Technology Think Tank Young Talent Program and LIESMARS Special Research Funding. (Corresponding author: Chi Chen).

References

Abdollahi, M.R., Pourtakdoust, S.H., Nooshabadi, M.H.Y., Pishkenari, H.N., n.d. An improved multi-state constraint kalman filter for visual-inertial odometry.

Adamkiewicz, M., Chen, T., Caccavale, A., Gardner, R., Culbertson, P., Bohg, J., Schwager, M., 2022. Vision-only robot navigation in a neural radiance world. *IEEE Robot. Autom. Lett.* 7, 4606–4613. https://doi.org/10.1109/LRA.2022.3150497

Al-Kaff, A., Martín, D., García, F., Escalera, A. de la, María Armingol, J., 2018. Survey of computer vision algorithms and applications for unmanned aerial vehicles. *Expert Syst.* Appl. 92, 447–463. https://doi.org/10.1016/j.eswa.2017.09.033

Bloesch, M., Omari, S., Hutter, M., Siegwart, R., 2015. Robust visual inertial odometry using a direct EKF-based approach, in: *2015 IEEE/RSJ International Conference on Intelligent Robots and Systems (IROS)*. Presented at the 2015 IEEE/RSJ International Conference on Intelligent Robots and Systems (IROS), IEEE, Hamburg, Germany, pp. 298–304. https://doi.org/10.1109/IROS.2015.7353389

Chen, C., Jin, A., Yang, B., Ma, R., Sun, S., Wang, Z., Zong, Z., Zhang, F., 2022. DCPLD-net: A diffusion coupled convolution neural network for real-time power transmission lines detection from UAV-borne LiDAR data. *Int. J. Appl. Earth Obs. Geoinformation* 112, 102960. https://doi.org/10.1016/j.jag.2022.102960

Chen, N., Kong, F., Xu, W., Cai, Y., Li, H., He, D., Qin, Y., Zhang, F., 2023. A self-rotating, single-actuated UAV with extended sensor field of view for autonomous navigation. *Sci. Robot.* 8. https://doi.org/10.1126/scirobotics.ade4538

Cheng, D., Ojeda, F.C., Prabhu, A., Liu, X., Zhu, A., Green, P.C., Ehsani, R., Chaudhari, P., Kumar, V., 2023. TreeScope: An agricultural robotics dataset for LiDAR-based mapping of trees in forests and orchards.

Cui, C., Shao, Q., Liu, Y., Han, G., Liu, F., Han, X., 2023. A review of the evolution and trends in research on the emergency evacuation of urban underground spaces. *Buildings* 13, 1325. https://doi.org/10.3390/buildings13051325

Deng, L., Mao, Z., Li, X., Hu, Z., Duan, F., Yan, Y., 2018. UAV-based multispectral remote sensing for precision agriculture: A comparison between different cameras. *ISPRS J. Photogramm. Remote Sens.* 146, 124–136. https://doi.org/10.1016/j.isprsjprs.2018.09.008

Gao, F., Wang, L., Zhou, B., Zhou, X., Pan, J., Shen, S., 2020. Teach-repeat-replan: A complete and robust system for aggressive flight in complex environments. *IEEE Trans. Robot.* 36, 1526–1545. https://doi.org/10.1109/TRO.2020.2993215

Geneva, P., Eckenhoff, K., Yang, Y., Huang, G., 2018. LIPS: LiDAR-inertial 3D plane SLAM, in: *2018 IEEE/RSJ International Conference on Intelligent Robots and Systems (IROS).* Presented at the 2018 IEEE/RSJ International Conference on Intelligent Robots and Systems (IROS), IEEE, Madrid, pp. 123–130. https://doi.org/10.1109/IROS.2018.8594463

Gentil, C.L., Vidal-Calleja, T., Huang, S., 2019. IN2LAMA: INertial lidar localisation and MApping, in: *2019 International Conference on Robotics and Automation (ICRA).* Presented at the 2019 International Conference on Robotics and Automation (ICRA), IEEE, Montreal, QC, Canada, pp. 6388–6394. https://doi.org/10.1109/ICRA.2019.8794429

Hunt, E.B., 2014. Artificial intelligence. *Academic Press*.

Kong, F., Xu, W., Zhang, F., 2021. Avoiding dynamic small obstacles with onboard sensing and computating on aerial robots.

Lai, Y., Wang, Y., Cheng, J., Chen, X., Liu, Q., 2023. Review of constraints and critical success factors of developing urban underground space. *Undergr. Space* 12, 137–155. https://doi.org/10.1016/j.undsp.2023.03.001

Leutenegger, S., Lynen, S., Bosse, M., Siegwart, R., Furgale, P., 2015. Keyframe-based visual–inertial odometry using nonlinear optimization. *Int. J. Robot. Res.* 34, 314–334. https://doi.org/10.1177/0278364914554813

Lin, Y., Gao, F., Qin, T., Gao, W., Liu, T., Wu, W., Yang, Z., Shen, S., 2018. Autonomous aerial navigation using monocular visual-inertial fusion. *J. Field Robot.* 35, 23–51. https://doi.org/10.1002/rob.21732

Mohta, K., Watterson, M., Mulgaonkar, Y., Liu, S., Qu, C., Makineni, A., Saulnier, K., Sun, K., Zhu, A., Delmerico, J., Karydis, K., Atanasov, N., Loianno, G., Scaramuzza, D., Daniilidis, K., Taylor, C.J., Kumar, V., 2018. Fast, autonomous flight in GPS-denied and cluttered environments. *J. Field Robot.* 35, 101–120. https://doi.org/10.1002/rob.21774

Mourikis, A.I., Roumeliotis, S.I., 2007. A multi-state constraint kalman filter for vision-aided inertial navigation, in: *Proceedings 2007 IEEE International Conference on Robotics and Automation.* Presented at the 2007 IEEE International Conference on Robotics and Automation, IEEE, Rome, Italy, pp. 3565–3572. https://doi.org/10.1109/ROBOT.2007.364024

Mur-Artal, R., Tardos, J.D., 2017. Visual-inertial monocular SLAM with map reuse. *IEEE Robot. Autom. Lett.* 2, 796–803. https://doi.org/10.1109/LRA.2017.2653359

Rouček, T., Pecka, M., Čížek, P., Petříček, T., Bayer, J., Šalanský, V., Heřt, D., Petrlík, M., Báča, T., Spurný, V., Pomerleau, F., Kubelka, V., Faigl, J., Zimmermann, K., Saska, M., Svoboda, T., Krajník, T., 2020. DARPA subterranean challenge: Multi-robotic exploration of underground environments, in: Mazal, J., Fagiolini, A., Vasik, P. (Eds.), Modelling and Simulation for Autonomous Systems, Lecture Notes in Computer Science. *Springer International Publishing, Cham,* pp. 274–290. https://doi.org/10.1007/978-3-030-43890-6_22

Sauro, F., Pozzobon, R., Massironi, M., De Berardinis, P., Santagata, T., De Waele, J., 2020. Lava tubes on earth, moon and mars: A review on their size and morphology revealed by comparative planetology. *Earth-Sci. Rev.* 209, 103288. https://doi.org/10.1016/j.earscirev.2020.103288

Sun, S., Chen, C., Wang, Z., Zhou, J., Li, L., Yang, B., Cong, Y., Wang, H., 2023. Real-time uav 3D image point clouds mapping. *ISPRS Ann. Photogramm. Remote Sens. Spat. Inf. Sci*. X-1/W1-2023, 1097–1104. https://doi.org/10.5194/isprs-annals-X-1-W1-2023-1097-2023

Sun, S., Cioffi, G., de Visser, C., Scaramuzza, D., 2020. Autonomous quadrotor flight despite rotor failure with onboard vision sensors: Frames vs. Events 8.

Tang, B., Ren, Y., Zhu, F., He, R., Liang, S., Kong, F., Zhang, F., 2023. Bubble explorer: Fast UAV exploration in large-scale and cluttered 3D-environments using occlusion-free spheres.

Tranzatto, M., Mascarich, F., Bernreiter, L., Godinho, C., Camurri, M., Khattak, S., Dang, T., Reijgwart, V., Löje, J., Wisth, D., Zimmermann, S., Nguyen, H., Fehr, M., Solanka, L., Buchanan, R., Bjelonic, M., Khedekar, N., Valceschini, M., Jenelten, F., Dharmadhikari, M., Homberger, T., De Petris, P., Wellhausen, L., Kulkarni, M., Miki, T., Hirsch, S., Montenegro, M., Papachristos, C., Tresoldi, F., Carius, J., Valsecchi, G., Lee, J., Meyer, K., Wu, X., Nieto, J., Smith, A., Hutter, M., Siegwart, R., Mueller, M., Fallon, M., Alexis, K., 2022. CERBERUS: Autonomous legged and aerial robotic exploration in the tunnel and urban circuits of the DARPA subterranean challenge. *Field Robot.* 2, 274–324. https://doi.org/10.55417/fr.2022011

von Stumberg, L., Usenko, V., Cremers, D., 2018. Direct sparse visual-inertial odometry using dynamic marginalization, in: *2018 IEEE International Conference on Robotics and Automation (ICRA).* pp. 2510–2517. https://doi.org/10.1109/ICRA.2018.8462905

Wan, E.A., n.d. The unscented kalman filter for nonlinear estimation.

Xiao, K., Tan, S., Wang, G., An, X., Wang, Xiang, Wang, Xiangke, 2020. XTDrone: A customizable multi-rotor UAVs simulation platform, in: *2020 4th International Conference on Robotics and Automation Sciences (ICRAS)*. Presented at the 2020 4th International Conference on Robotics and Automation Sciences (ICRAS), IEEE, Wuhan, China, pp. 55–61. https://doi.org/10.1109/ICRAS49812.2020.9134922

Xiao L., Huang J., Zhao JiaWei, Zhao JianNan, 2018. Significance and preliminary proposal for exploring the lunar lava tubes. *Sci. Sin. Phys. Mech. Astron.* 48, 119602. https://doi.org/10.1360/SSPMA2018-00025

Yu, P., Liu, H., Wang, Z., Fu, J., Zhang, H., Wang, J., Yang, Q., 2023. Development of urban underground space in coastal cities in China: A review. *Deep Undergr. Sci. Eng.* 2, 148–172. https://doi.org/10.1002/dug2.12034

Zhang, J., Singh, S., 2014. LOAM: Lidar odometry and mapping in real-time, in: Robotics: Science and Systems X. Presented at the *Robotics: Science and Systems* 2014, Robotics: Science and Systems Foundation. https://doi.org/10.15607/RSS.2014.X.007

Zhou, B., Gao, F., Pan, J., Shen, S., 2020. Robust real-time UAV replanning using guided gradient-based optimization and topological paths.

Zhou, B., Pan, J., Gao, F., Shen, S., 2021. RAPTOR: Robust and perception-aware trajectory replanning for quadrotor fast flight. *IEEE Trans. Robot.* 37, 1992–2009. https://doi.org/10.1109/TRO.2021.3071527

Zhou, X., Wang, Z., Ye, H., Xu, C., Gao, F., 2020. EGO-planner: An ESDF-free gradient-based local planner for quadrotors. ArXiv200808835 Cs.

Zhou, X., Wen, X., Wang, Z., Gao, Y., Li, H., Wang, Q., Yang, T., Lu, H., Cao, Y., Xu, C., Gao, F., 2022. Swarm of micro flying robots in the wild. *Sci. Robot.* 7, eabm5954. https://doi.org/10.1126/scirobotics.abm5954